Geochemical Perspectives Letters

Titanium isotope constraints on the mafic sources and geodynamic origins of Archean crust

L. Hoare[1*], L.J.A. Rzehak[1,2], S. Kommescher[1,2], M. Jansen[3], M.T. Rosing[4], T. Nagel[5], M.-A. Millet[6], J.E. Hoffmann[7], R.O.C. Fonseca[1]

OPEN ACCESS
https://doi.org/10.7185/geochemlet.2342

Abstract

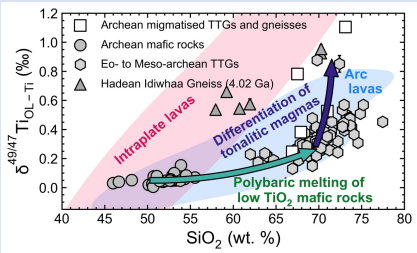

The timing and formation of Earth's first continents during the Archean are subjects of significant debate. By examining titanium isotope variations in Archean Tonalite-Trondhjemite-Granodiorite (TTG) rocks and using advanced thermodynamic modelling, we can narrow down the processes involved and emphasise the role of mafic precursor compositions. In our study of Eoarchean Isua metabasalts and Itsaq tonalites in southern West Greenland, we observed a pattern of increasing Ti isotope enrichment with higher SiO_2 content, resembling the compositions found in modern subduction zone rocks. Our modelling suggests that the Ti isotope variations in TTGs can be best explained by a combination of partial melting of low TiO_2 metabasalts and subsequent crystallisation of tonalitic magmas, resulting in heavier Ti isotopes. This means that Ti isotopes help us distinguish the contributions of various mafic sources and fractional crystallisation during TTG formation. In the case of Itsaq tonalites and many other Eoarchean TTGs, low TiO_2 tholeiitic metabasalts with arc-like characteristics likely represent the mafic source rocks, suggesting the formation of some of Earth's earliest continental crust within a proto-subduction zone setting.

Received 22 June 2023 | Accepted 6 November 2023 | Published 22 December 2023

Introduction

Remnants of Archean juvenile continental crust are preserved in the form of sodic granitoids collectively known as Tonalite-Trondhjemite-Granodiorites (TTG). There is ongoing debate about the origin of these incomplete remnants, leading to varying interpretations over the responsible tectonic regime. TTG formation hypotheses are broadly divided between two end members that involve partial melting of thickened, hydrated mafic crust in 1) a horizontal tectonic regime, possibly analogous to modern subduction (*e.g.*, Foley *et al.*, 2002), or 2) a non-uniformitarian regime such as oceanic plateaux (*e.g.*, Nair and Chacko, 2008). Furthermore, despite extensive geochemical and experimental evidence supporting polybaric dehydration melting of hydrated mafic crust as a formation mechanism of juvenile TTG magmas (*e.g.*, Barker and Arth, 1976; Rapp *et al.*, 1991), many TTGs have undergone subsequent fractional crystallisation (*e.g.*, Laurent *et al.*, 2020), obscuring the nature of their mafic protolith.

Mass dependent isotope variations of titanium (expressed as $\delta^{49/47}$Ti) have recently been utilised as a novel tool to investigate magmatic differentiation (Millet *et al.*, 2016; Greber *et al.*, 2017; Deng *et al.*, 2019; Aarons *et al.*, 2020; Hoare *et al.*, 2020), and can be applied to test petrogenetic models of TTG formation. Based on these studies it has been postulated that titanium isotope fractionation is mainly driven by the sequestration of light isotopes into Fe-Ti oxides (ilmenite, magnetite, and rutile) where Ti occupies VI-fold coordination (*e.g.*, Hoare *et al.*, 2022; Johnson *et al.*, 2023). Consequently, melts in equilibrium with these phases are enriched in heavy Ti isotopes, which occupy lower coordination (VI- and V-fold). Furthermore, $\delta^{49/47}$Ti variations of evolved magmas from different geodynamic settings show differences (Fig. 1). Silicic melts from reduced, H_2O-poor, Ti-rich intra-plate magmas have higher $\delta^{49/47}$Ti relative to arc magmas at a given SiO_2 content (Fig. 1; Deng *et al.*, 2019; Hoare *et al.*, 2020). In alkaline intra-plate magmas, larger Ti isotope fractionation is driven by significant Fe-Ti oxide crystallisation, in contrast to hydrous subduction zone magmas where only low Ti magnetite is present (Hoare *et al.*, 2022; Johnson *et al.*, 2023). The uniform Ti isotope composition in Archean shales and comparable fractionation patterns in Archean TTGs have sparked the hypothesis that substantial felsic crust has existed since 3.5 billion years ago, potentially indicating past plate tectonics (Greber *et al.*, 2017; Zhang *et al.*, 2023). Conversely, non-subduction related magmatism also produces felsic rocks with heavy Ti isotope

1. Institut für Geologie, Mineralogie und Geophysik, Ruhr-Universität Bochum, 150 Universitätsstraße, 44801 Bochum, Germany
2. Institut für Geologie und Mineralogie, Universität Zu Köln, Zülpicher Str. 49b, 50674, Cologne, Germany
3. Deutsches Bergbau-Museum Bochum, Leibniz-Research Museum for Georesources, Herner Str. 45, 44787 Bochum, Germany
4. Globe Institute, University of Copenhagen, Øster Voldgade 5-7, 1350 København, Denmark
5. Institut für Geologie, Technische Universität Bergakademie Freiberg, Bernhard-von-Cotta-Str. 209599 Freiberg, Germany
6. School of Earth and Environmental Sciences, Cardiff University, Main Building, Park Place, Cardiff CF10 3AT, UK
7. Institut für Geologische Wissenschaften, Freie Universität Berlin, Malteserstraße 74-100, 12249 Berlin, Germany
* Corresponding author (email: liam.hoare@rub.de)

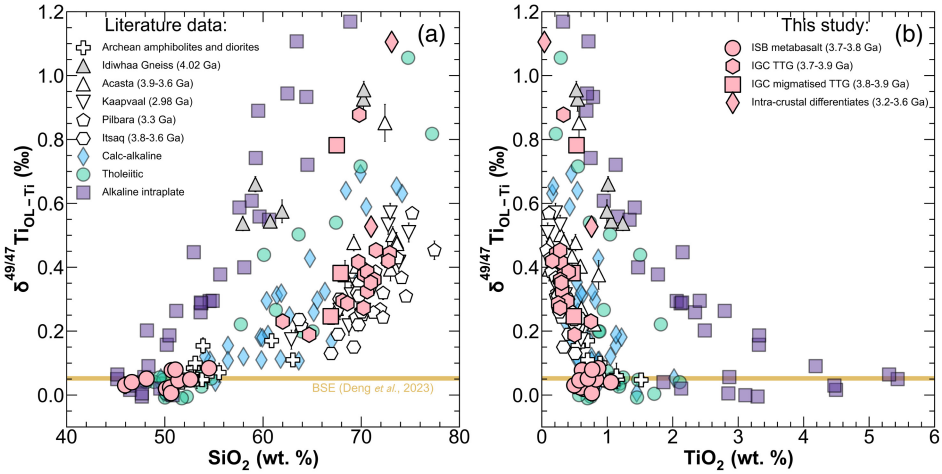

Figure 1 $\delta^{49/47}$Ti compositions of ISB metabasalts, IGC tonalites and intra-crustal differentiates, with other Hadean-Archean rocks, compared to Phanerozoic lavas from different tectonic settings *versus* **(a)** SiO_2 and **(b)** TiO_2. Literature sources are given in the Supplementary Information, Table S-11.

compositions (Deng *et al.*, 2019) and the Ti isotope composition of sedimentary archives may be biased *via* mechanical processes (Klaver *et al.*, 2021; Saji *et al.*, 2023). These factors challenge the reliability of Archean sediments as Ti isotope archives of the continental crust. A subsequent study by Aarons *et al.* (2020) observed that SiO_2 *vs.* $\delta^{49/47}$Ti covariations within 4.02 Ga Idiwhaa gneisses from the Acasta Gneiss Complex, Slave craton, Canada (Fig. 1a), mirror the trend of alkaline intra-plate magmas, whereas post-4.02 Ga TTGs exhibit $\delta^{49/47}$Ti variations comparable to modern calc-alkaline magmas (Aarons *et al.*, 2020). This dichotomy may imply a transition to subduction style tectonics at the Hadean-Archean boundary (Aarons *et al.*, 2020). The usefulness of Ti isotopes in understanding early Earth geodynamics is challenging due to the lack of information about Hadean mafic crust composition (Nebel *et al.*, 2014) and differing opinions on the ideal mafic protolith for Archean TTG magmas (Smithies *et al.*, 2009; Nagel *et al.*, 2012). Accurate knowledge of mafic protoliths is crucial because the early Archean mantle had a distinct Ti isotope composition from today (Deng *et al.*, 2023), and the composition of the parental melt significantly influences Ti isotope fractionation during magmatic processes (Deng *et al.*, 2019; Hoare *et al.*, 2020). Elucidating the composition of the mafic protolith may thus provide tighter constraints of the geodynamic setting of TTG formation.

Here we present $\delta^{49/47}$Ti data of well characterised Eoarchean (3.8–3.7 Ga) tholeiitic metabasalts from the Isua supracrustal belt (ISB) and Palaeo- to Eoarchean (3.9–3.2 Ga) tonalites and intra-crustal differentiates (pegmatites and augen gneisses) from the adjacent Itsaq Gneiss Complex (IGC) of southern West Greenland. The Itsaq meta-tonalites are found within low-strain zones in the IGC as almost undeformed, single phase tonalites with partially preserved primary magmatic textures and mineral assemblages (Nutman *et al.*, 1999) making these samples ideal to investigate early crustal formation. These rocks are interpreted to originate from polybaric partial melting of thickened, arc-like mafic crust followed by fractional crystallisation of pooled melts in mid-crustal plutons, within a geodynamic regime analogous to a modern subduction setting (Nagel *et al.*, 2012; Hoffmann *et al.*, 2014). Others argue against such an origin, favouring non-uniformitarian processes (Rollinson, 2022). We use Ti isotope variations in ISB and IGC rocks, and detailed thermodynamic modelling, to unravel the influence of mafic source composition and the effects of partial melting and crystallisation processes on the geochemistry of Archean TTGs.

Results

Titanium isotope measurements are reported as $\delta^{49/47}Ti_{OL\text{-}Ti}$ (‰) = $[^{49/47}Ti_{sample}/^{49/47}Ti_{OL\text{-}Ti} - 1] * 10^3$, which is the deviation in parts *per* thousand of the $^{49}Ti/^{47}Ti$ ratio relative to Origins Laboratory Ti (OL-Ti), the recognised Ti reference material. The $\delta^{49/47}$Ti values of ISB tholeiitic metabasalts show limited variation (+0.01 to +0.09 ‰). Non-gneissic IGC tonalites display $\delta^{49/47}$Ti compositions between +0.18 and +0.88 ‰ (Fig. 1). Migmatised tonalites and intra-crustal differentiates (augen and pegmatitic gneisses) also show substantial variability in δ^{49}Ti; +0.25 to +0.78 ‰, and +0.55 to +1.11 ‰, respectively. To assess the extent of Ti isotope fractionation during partial melting of different mafic source compositions and magmatic differentiation we utilise constraints from thermodynamic phase equilibria modelling combined with relevant mineral-melt Ti isotope fractionation factors. A detailed summary of our results and modelling are provided in the Supplementary Information.

Ti Isotope Fractionation During Partial Melting of Different Mafic Protoliths

Polybaric melting of a single mafic source has been invoked to explain the chemical diversity of TTG magmas. However, given the sensitivity of Ti isotope fractionation to parental melt composition (Deng *et al.*, 2019; Hoare *et al.*, 2020), partial melting of diverse mafic sources of differing TiO_2 contents will likely generate melts with contrasting Ti isotope compositions. Polybaric melting of both TiO_2-poor (~0.6–0.7 wt. %) Isua tholeiitic metabasalts, and intermediate TiO_2 (~1 wt. %) plateau basalts produce tonalitic melts (SiO_2 > 60 wt. %) with $\delta^{49/47}$Ti between ~+0.10 to +0.26 ‰ (Fig. 2). The partial melt compositions in these scenarios define shallow trends of increasing $\delta^{49/47}$Ti with increasing SiO_2 and decreasing TiO_2 (Fig. 2a). For low Al metabasalts, the absence of residual plagioclase means that, at a given melt fraction and $\delta^{49/47}$Ti, melt compositions are shifted to lower SiO_2 (Fig. 2a). Low pressure (0.8 GPa) melting of E-MORB (~1.5 wt. % TiO_2), produces a steep trend with elevated $\delta^{49/47}$Ti at lower SiO_2 and higher TiO_2 (Fig. 2b). Melting E-MORB at higher pressure (1.3 GPa) produces a notably shallower trend. However, irrespective of melting pressure, higher TiO_2 mafic sources produce melt compositions that are generally too TiO_2-rich at a given SiO_2 content (Fig. 2b,d). Conversely, the

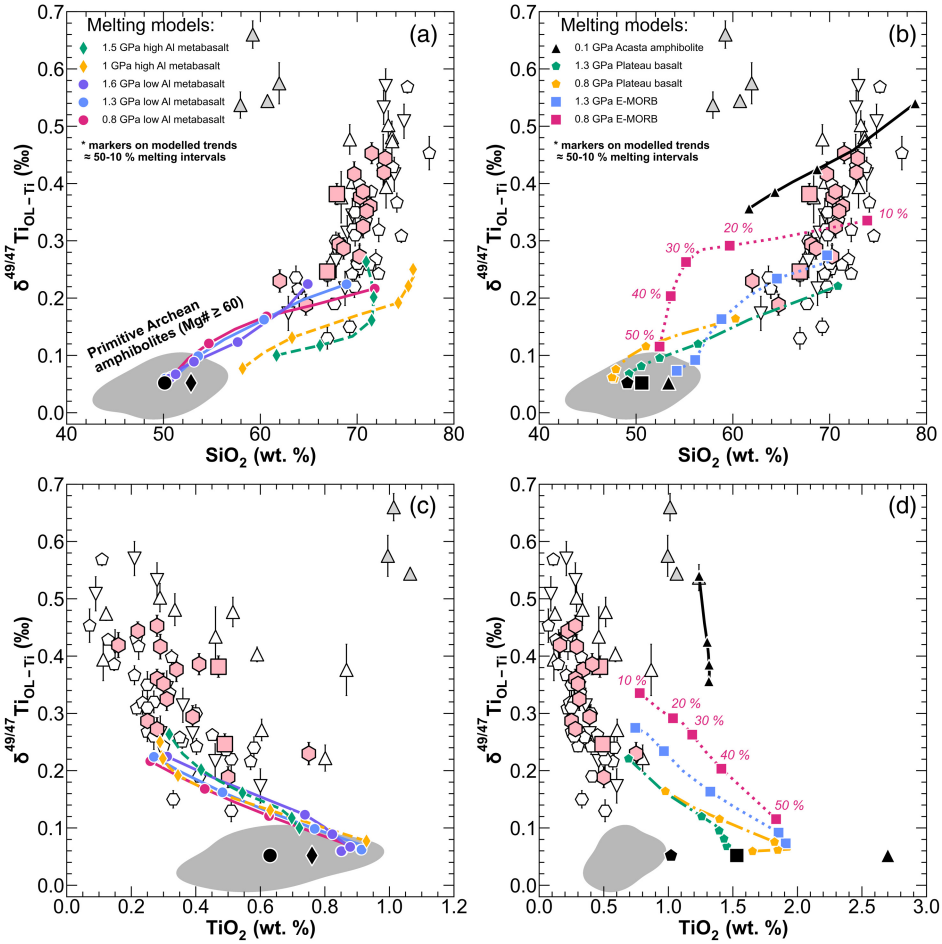

Figure 2 $\delta^{49/47}$Ti *versus* SiO_2 and TiO_2 for partial melting of high and low Al Isua metabasalts at 0.8–1.6 GPa **(a and c)**; and partial melting of E-MORB and primitive plateau basalt at 0.8–1.3 GPa **(b and d)** superimposed on to $\delta^{49/47}$Ti data for Hadean-Archean TTGs (pink, white and grey symbols; see Fig. 1 for the legend). Shaded grey field represents $\delta^{49/47}$Ti range of primitive Archean amphibolites (Mg# > 60) defined by a 0.95 probability density contour. Black symbols indicate the starting composition for each model. Symbols on modelled trends represent melting intervals between 50–10 %. Modelling details are given in the Supplementary Information.

impact melt scenario of Johnson *et al.* (2018) for the Hadean Idiwhaa gneisses, would involve low pressure (0.1 GPa) melting of a TiO_2-rich protolith (~2.7 wt. %) producing amphibole-free residues and high SiO_2-TiO_2 melts with significantly higher $\delta^{49/47}$Ti (~+0.36 to +0.54 ‰) relative to the other melting scenarios (Fig. 2b,d). However, it is noteworthy that this model produces, at best, an imperfect match to the Idiwhaa data (Fig. 2b,d). The varying magnitude of Ti isotope fractionation during partial melting is largely driven by competition between amphibole and Fe-Ti oxides for the elemental budget of Ti (Fig. S-1; Supplementary Information). Amphibole is the dominant Ti-bearing phase during melting of low to intermediate Ti mafic sources, whereas Fe-Ti oxides, which possess larger Ti isotope fractionation factors, are mostly absent (Fig. S-1; Supplementary Information). Higher parental melt TiO_2 contents enable greater abundances of Fe-Ti oxides in the melting residues (Fig. S-1). This results in a greater magnitude of Ti isotope fractionation (Fig. 2), with reduced fractionation at higher pressure as rutile possesses a smaller fractionation factor relative to ilmenite (Hoare *et al.*, 2022; Rzehak *et al.*, 2022). Therefore, the shallow positive correlation between $\delta^{49/47}$Ti and SiO_2 shared by modern calc-alkaline lavas and Archean TTGs (Fig. 1a) could be largely coincidental, with the modest fractionation in TTGs reflecting the dominance of amphibole on the Ti budget during partial melting. Furthermore, the dominant role of amphibole likely precludes a TiO_2 -rich (>1 wt. %) mafic source for Itsaq tonalites and other Eoarchean TTGs or requires very low or high melting pressures if TiO_2-rich mafic sources are invoked (Fig. 2). Nevertheless, polybaric melting of low-TiO_2 metabasalts can only reproduce the $\delta^{49/47}$Ti variation for TTGs with $\delta^{49/47}$Ti up to ~+0.3 ‰ (Fig. 2a,c), suggesting that an additional process is required to explain $\delta^{49/47}$Ti above that value.

Ti Isotope Fractionation During Magmatic Differentiation and Crustal Re-Working

While partial melting of tholeiitic metabasalts accounts for many major and trace element characteristics of IGC tonalites (cf. Hoffmann *et al.*, 2014), our modelling reveals that partial melting alone cannot reproduce the complete range of $\delta^{49/47}$Ti in TTGs (Fig. 2). The differentiation of intermediate tonalitic/andesitic liquids is fundamental to generating evolved magmas within the Earth's crust (*e.g.*, Marxer and Ulmer, 2019), and similar processes have been invoked to explain the compositional diversity of TTG magmas (*e.g.*, Laurent *et al.*, 2020).

Equilibrium crystallisation models of tonalitic magmas (~62–66 wt. % SiO_2) at 0.5 GPa with an initial $\delta^{49/47}$Ti ranging between ~+0.2 to +0.3 ‰ produces evolved melts (>70 wt. % SiO_2) with $\delta^{49/47}$Ti values up to ~+0.6 ‰ (Fig. 3). Fractional crystallisation at the same pressure produces TTG melts with heavier

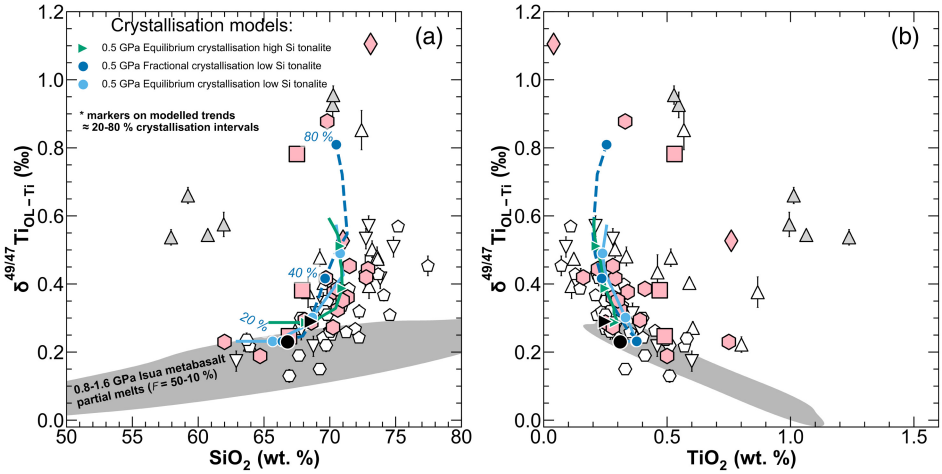

Figure 3 $\delta^{49/47}$Ti *versus* **(a)** SiO_2 and **(b)** TiO_2 for equilibrium (solid lines) and fractional crystallisation (dashed line) of tonalitic melts at 0.5 GPa compared to $\delta^{49/47}$Ti of Hadean-Archean TTGs (pink, white and grey symbols; see Fig. 1 for legend). Shaded grey field represents the $\delta^{49/47}$Ti range of modelled 50–10 % partial melts of Isua metabasalts from Figure 2 defined by a 0.95 probability density contour. Black symbols indicate the starting composition for each model. Symbols on modelled trends represent crystallisation intervals between 20–80 %. Modelling details are given in the Supplementary Information.

$\delta^{49/47}$Ti up to +0.8 ‰ (Fig. 3). Titanium isotope fractionation during differentiation of tonalitic magmas is largely controlled by ilmenite, and to a lesser extent, amphibole, and biotite. Consequently, at a given temperature, the bulk Ti solid-melt fractionation factor ($\alpha_{solid\text{-}melt}$) is larger for crystallisation compared to partial melting, where amphibole has a greater influence on $\alpha_{solid\text{-}melt}$ (Supplementary Information). Equilibrium crystallisation is responsible for most of the $\delta^{49/47}$Ti variation in IGC tonalites and other Archean TTGs, spanning approximately +0.3 to +0.6 ‰ (as seen in Fig. 2d). This process likely occurred within upper crustal crystal mushes, as suggested by Laurent *et al.* (2020). The scatter of some TTGs with $\delta^{49/47}$Ti > +0.3 ‰ (Fig. 3) can be explained by differentiation of tonalitic magmas of differing initial SiO_2 and TiO_2 contents, themselves the products of variable polybaric melting (Fig. 2).

There is an additional complication that migmatised IGC tonalites and intra-crustal differentiates generally exhibit more scatter in their $\delta^{49/47}$Ti compositions compared to non-gneissic tonalites, with elevated $\delta^{49/47}$Ti at lower SiO_2 and higher TiO_2 (Figs. 2, 3). Furthermore, intra-crustal differentiates display significantly heavier Ti isotope compositions above +1 ‰ (Figs. 2, 3). These samples are characterised by superchondritic Nb/Ta (21–37), suggesting the fractionation of Ti-bearing phases like rutile, titanite or ilmenite (Hoffmann *et al.*, 2011). Moreover, these samples were identified in the field as being amphibolite facies rocks that had previously experienced prior modification by melts or fluids (Nutman and Bridgwater, 1986). Given that intra-crustal differentiates are ~200 Myr younger than the majority of Istaq TTGs, the scatter in $\delta^{49/47}$Ti could result from a subsequent intra-crustal melting event where additional Ti isotope fractionation was driven by rutile or ilmenite. Intra-crustal melting might have resulted from crustal thickening, causing the remelting of pre-existing felsic, likely isotopically heavy, portions of the lower continental crust. These high Nb/Ta felsic melts could have then infiltrated the mid-crust (Hoffmann *et al.* 2011).

The Influence of Source Depth on the Ti Isotope Evolution of TTG Magmas

Based on $\delta^{49/47}$Ti systematics alone it is difficult to fully establish the control of melting pressure, which dictates the stable phase assemblages during partial melting. However, the full spectrum of variations in trace element ratios (*e.g.*, Zr/Sm, Gd/Yb and Nb/Ta) in IGC tonalites implies the presence of garnet and a Ti-bearing phase (such as rutile or ilmenite) in the melting residuum, and hence polybaric melting (*e.g.*, Nagel *et al.*, 2012; Hoffmann *et al.*, 2014). Dy/Dy* is an effective discriminator for the roles of amphibole, garnet, and source LREE (Light Rare Earth Element) contents in magmatic processes (Davidson *et al.*, 2013). When combined with phase equilibria modelling it can provide quantitative estimates on source mineralogy and melting depth during TTG formation (Fig. 4). The negative correlation between Dy/Dy* and $\delta^{49/47}$Ti is evidence of the dominant role for amphibole in dictating the $\delta^{49/47}$Ti composition of TTGs (Fig. 4). The majority of Eoarchean TTGs with $\delta^{49/47}$Ti < +0.3 ‰ do not require melting pressures greater than 1.6 GPa if low TiO_2, LREE-enriched metabasalts are invoked as the source (Fig. 4a). Conversely, E-MORB or primitive plateau basalt are slightly too enriched or depleted, respectively, to fully encapsulate the natural TTG data at 0.8–1.3 GPa (Fig. 4b). The absence of a significant negative Dy/Dy* for the Idiwhaa gneisses suggests a reduced role for amphibole and thus their higher $\delta^{49/47}$Ti are primarily influenced by Fe-Ti oxides. The $\delta^{49/47}$Ti-Dy/Dy* systematics indicates that the formation of Eoarchean TTGs may not require high pressure eclogite facies conditions (≥2 GPa) for partial melting. This challenges previous proposals, such as those by Rapp *et al.* (2003), that suggested high pressure conditions were required to produce juvenile continental crust.

Geodynamic Implications of Ti Isotope Variations in TTGs

Our study reveals that the formation of most Eoarchean TTG magmas likely included low to medium pressure melting of low TiO_2, REE-enriched metabasalts, followed by differentiation of tonalitic melts within upper crustal crystal mushes, resulting in TTGs with higher $\delta^{49/47}$Ti values. The shallow positive correlation between $\delta^{49/47}$Ti and SiO_2 shared by modern calc-alkaline lavas and Archean TTGs may be coincidental, rather reflecting the dominance of amphibole over Fe-Ti oxides during partial melting. Partial melts of TiO_2-rich mafic protoliths result in melts with elevated $\delta^{49/47}$Ti at a given SiO_2 and TiO_2 compared to most Eoarchean TTGs, unless melting occurs at either very low (0.1 GPa) or higher pressures (>1.3 GPa). Consequently, this

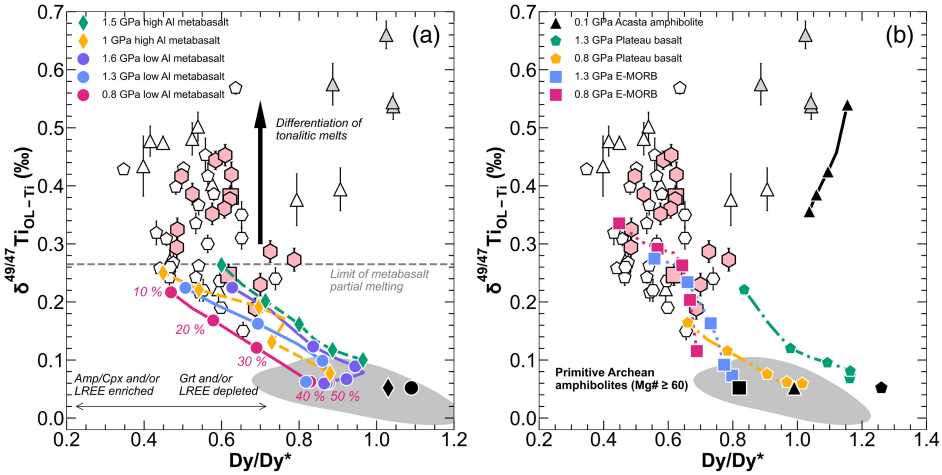

Figure 4 $\delta^{49/47}$Ti *versus* Dy/Dy* (after Davidson *et al.*, 2013) for partial melting of **(a)** high and low Al Isua metabasalts at 0.8–1.6 GPa, and **(b)** partial melting of E-MORB and primitive plateau basalt at 0.8–1.3 GPa superimposed on to $\delta^{49/47}$Ti data for Hadean-Archean TTGs (pink, white and grey symbols, refer to Fig. 1 for the symbol legend). Shaded grey field represents the $\delta^{49/47}$Ti range of primitive Archean amphibolites (Mg# > 60) defined by a 0.95 probability density contour. Black symbols indicate the starting composition for each model. Symbols on modelled trends represent melting intervals between 50–10 %. Modelling details are given in the Supplementary Information.

rules out a TiO_2-rich mafic source and a plume origin for most Eoarchean TTGs. The $\delta^{49/47}$Ti systematics of the Hadean Idiwhaa gneisses necessitate a TiO_2-rich source and potentially an intraplate origin (Aarons *et al.*, 2020); however, the mechanism responsible for their heavy Ti compositions could have plausibly resulted from a combination of very low pressure melting (Johnson *et al.*, 2018) and fractional crystallisation (Aarons *et al.*, 2020). In the case of the Eoarchean Itsaq tonalites, the chemistry of their mafic sources resembles modern tholeiitic arc basalts, suggesting a potential subduction origin (*e.g.*, Jenner *et al.*, 2009). If subduction did indeed occur in the Eoarchean, it is likely not comparable to the present day (Sizova *et al.*, 2015), and was mostly at or below garnet-amphibolite facies conditions (~1–1.5 GPa; *e.g.*, Zhang *et al.*, 2013). The Ti isotope systematics of Eoarchean Itsaq tonalites are consistent with formation within a 'proto-subduction zone' (*e.g.*, Hoffmann *et al.*, 2014). In this scenario, low to medium pressure melting of hydrated low TiO_2 arc-like mafic crust is triggered *via* crustal thickening due to successive tholeiitic intrusions, which results in destabilisation and overturn of crustal fragments (*e.g.*, Sizova *et al.*, 2015). It is worth noting that Ti isotopes are better suited to distinguish between mafic sources and petrogenetic processes during crustal formation rather than direct proxies for tectonic settings. For instance, it cannot be ruled out that melting of low TiO_2 basalts may have occurred within subducted or thickened oceanic plateaux (Nair and Chacko, 2008; Johnson *et al.*, 2017). Thus, the sentiment that the full spectrum of Archean TTGs may have formed from various geodynamic settings and mafic sources cannot be completely discounted, and any such inferences need to be made on a more regional scale.

Acknowledgements

LH, ROCF, and JEH acknowledge funding from Deutsche Forschungsgemeinschaft (DFG) Grant FO 698/14-1 and HO4794/4-1. ROC further thanks the DFG for funding of a Heisenberg Professorship (Grant FO 698/13-1). We thank Regina Friese and Michael Bode for managing the clean lab at the Deutches Bergbau Museum, and Edward Inglis for managing the clean lab at Cardiff University. We also thank Philipp Gleißner, Ninja Braukmüller and Guillaume Florin for assistance and advice with the Neoma MC-ICP-MS at Freie Universität Berlin. We thank Carsten Münker and Kristoffer Szilas for providing access to additional samples, and in the case of the former, access to laboratory facilities at the University of Cologne during the preliminary stages of this project. We are grateful to Silvia Volante and Capucine Albert for helpful discussions. The authors would also like to acknowledge detailed and constructive reviews by two anonymous referees which greatly improved the manuscript. Furthermore, we would like to thank Anat Shahar for expert editorial handling.

Editor: Anat Shahar

Additional Information

Supplementary Information accompanies this letter at https://www.geochemicalperspectivesletters.org/article2342.

Cite this letter as: Hoare, L., Rzehak, L.J.A., Kommescher, S., Jansen, M., Rosing, M.T., Nagel, T., Millet, M.-A., Hoffmann, J.E., Fonseca, R.O.C. (2023) Titanium isotope constraints on the mafic sources and geodynamic origins of Archean crust. *Geochem. Persp. Let.* 28, 37–42. https://doi.org/10.7185/geochemlet.2342

References

Aarons, S.M., Reimink, J.R., Greber, N.D., Heard, A.W., Zhang, Z., Dauphas, N. (2020) Titanium isotopes constrain a magmatic transition at the Hadean-Archean boundary in the Acasta Gneiss Complex. *Science Advances* 6, eabc9959. https://doi.org/10.1126/sciadv.abc9959

Barker, F., Arth, J.G. (1976) Generation of trondhjemitic-tonalitic liquids and Archean bimodal trondhjemite-basalt suites. *Geology* 4, 596–600. https://doi.org/10.1130/0091-7613(1976)4%3C596:GOTLAA%3E2.0.CO;2

Davidson, J., Turner, S., Plank, T. (2013) Dy/Dy*: variations arising from mantle sources and petrogenetic processes. *Journal of Petrology* 54, 525–537. https://doi.org/10.1093/petrology/egs076

Deng, Z., Chaussidon, M., Savage, P., Robert, F., Pik, R., Moynier, F. (2019) Titanium isotopes as a tracer for the plume or island arc affinity of felsic rocks. *Proceedings of the National Academy of Sciences* 116, 1132–1135. https://doi.org/10.1073/pnas.1809164116

Deng, Z., Schiller, M., Jackson, M.G., Millet, M.-A., Pan, L., Nikolajsen, K., Saji, N.S., Huang, D., Bizzarro, M. (2023) Earth's evolving geodynamic regime recorded by titanium isotopes. *Nature* 621, 100–104. https://doi.org/10.1038/s41586-023-06304-0

Foley, S., Tiepolo, M., Vannucci, R. (2002) Growth of early continental crust controlled by melting of amphibolite in subduction zones. *Nature* 417, 837–840. https://doi.org/10.1038/nature00799

Greber, N.D., Dauphas, N., Bekker, A., Ptáček, M.P., Bindeman, I.N., Hofmann, A. (2017) Titanium isotopic evidence for felsic crust and plate tectonics 3.5 billion years ago. *Science* 357, 1271–1274. https://doi.org/10.1126/science.aan8086

Hoare, L., Klaver, M., Saji, N.S., Gillies, J., Parkinson, I.J., Lissenberg, C.J., Millet, M.-A. (2020) Melt chemistry and redox conditions control titanium isotope fractionation during magmatic differentiation. *Geochimica et Cosmochimica Acta* 282, 38–54. https://doi.org/10.1016/j.gca.2020.05.015

Hoare, L., Klaver, M., Muir, D.D., Klemme, S., Barling, J., Parkinson, I.J., Lissenberg, C.J., Millet, M.-A. (2022) Empirical and experimental constraints on Fe-Ti oxide-melt titanium isotope fractionation factors. *Geochimica et Cosmochimica Acta* 326, 253–272. https://doi.org/10.1016/j.gca.2022.02.011

Hoffmann, J.E., Münker, C., Næraa, T., Rosing, M.T., Herwartz, D., Garbe-Schönberg, D., Svahnberg, H. (2011) Mechanisms of Archean crust formation inferred from high-precision HFSE systematics in TTGs. *Geochimica et Cosmochimica Acta* 75, 4157–4178. https://doi.org/10.1016/j.gca.2011.04.027

Hoffmann, J.E., Nagel, T.J., Muenker, C., Naeraa, T., Rosing, M.T. (2014) Constraining the process of Eoarchean TTG formation in the Itsaq Gneiss Complex, southern West Greenland. *Earth and Planetary Science Letters* 388, 374–386. https://doi.org/10.1016/j.epsl.2013.11.050

Jenner, F., Bennett, V., Nutman, A., Friend, C., Norman, M., Yaxley, G. (2009) Evidence for subduction at 3.8 Ga: geochemistry of arc-like metabasalts from the southern edge of the Isua Supracrustal Belt. *Chemical Geology* 261, 83–98. https://doi.org/10.1016/j.chemgeo.2008.09.016

Johnson, A.C., Zhang, Z.J., Dauphas, N., Rudnick, R.L., Foden, J.D., Toc, M. (2023) Redox and mineral controls on Fe and Ti isotopic fractionations during calc-alkaline magmatic differentiation. *Geochimica et Cosmochimica Acta* 355, 1–12. https://doi.org/10.1016/j.gca.2023.06.016

Johnson, T.E., Brown, M., Gardiner, N.J., Kirkland, C.L., Smithies, R.H. (2017) Earth's first stable continents did not form by subduction. *Nature* 543, 239–242. https://doi.org/10.1038/nature21383

Johnson, T.E., Gardiner, N.J., Miljković, K., Spencer, C.J., Kirkland, C.L., Bland, P.A., Smithies, H. (2018) An impact melt origin for Earth's oldest known evolved rocks. *Nature Geoscience* 11, 795–799. https://doi.org/10.1038/s41561-018-0206-5

Klaver, M., MacLennan, S.A., Ibañez-Mejia, M., Tissot, F.L.H., Vroon, P.Z., Millet, M.-A. (2021) Reliability of detrital marine sediments as proxy for continental crust composition: The effects of hydrodynamic sorting on Ti and Zr isotope systematics. *Geochimica et Cosmochimica Acta* 310, 221–239. https://doi.org/10.1016/j.gca.2021.05.030

Laurent, O., Björnsen, J., Wotzlaw, J.-F., Bretscher, S., Pimenta Silva, M., Moyen, J.-F., Ulmer, P., Bachmann, O. (2020) Earth's earliest granitoids are crystal-rich magma reservoirs tapped by silicic eruptions. *Nature Geoscience* 13, 163–169. https://doi.org/10.1038/s41561-019-0520-6

Marxer, F., Ulmer, P. (2019) Crystallisation and zircon saturation of calc-alkaline tonalite from the Adamello Batholith at upper crustal conditions: an experimental study. *Contributions to Mineralogy and Petrology* 174, 84. https://doi.org/10.1007/s00410-019-1619-x

Millet, M.-A., Dauphas, N., Greber, N.D., Burton, K.W., Dale, C.W., Debret, B., Macpherson, C.G., Nowell, G.M., Williams, H.M. (2016) Titanium stable isotope investigation of magmatic processes on the Earth and Moon. *Earth and Planetary Science Letters* 449, 197–205. https://doi.org/10.1016/j.epsl.2016.05.039

Nagel, T.J., Hoffmann, J.E., Münker, C. (2012) Generation of Eoarchean tonalite-trondhjemite-granodiorite series from thickened mafic arc crust. *Geology* 40, 375–378. https://doi.org/10.1130/G32729.1

Nair, R., Chacko, T. (2008) Role of oceanic plateaus in the initiation of subduction and origin of continental crust. *Geology* 36, 583–586. https://doi.org/10.1130/G24773A.1

Nebel, O., Rapp, R.P., Yaxley, G.M. (2014) The role of detrital zircons in Hadean crustal research. *Lithos* 190, 313–327. https://doi.org/10.1016/j.lithos.2013.12.010

Nutman, A.P., Bridgwater, D. (1986) Early Archaean Amitsoq tonalites and granites of the Isukasia area, southern West Greenland: development of the oldest-known sial. *Contributions to Mineralogy and Petrology* 94, 137–148. https://doi.org/10.1007/s004100050556

Nutman, A.P., Bennett, V.C., Friend, C.R., Norman, M.D. (1999) Meta-igneous (non-gneissic) tonalites and quartz-diorites from an extensive ca. 3800 Ma terrain south of the Isua supracrustal belt, southern West Greenland: constraints on early crust formation. *Contributions to Mineralogy and Petrology* 137, 364–388. https://doi.org/10.1007/s004100050556

Rapp, R.P., Watson, E.B., Miller, C.F. (1991) Partial melting of amphibolite/eclogite and the origin of Archean trondhjemites and tonalites. *Precambrian Research* 51, 1–25. https://doi.org/10.1016/0301-9268(91)90092-O

Rapp, R.P., Shimizu, N., Norman, M.D. (2003) Growth of early continental crust by partial melting of eclogite. *Nature* 425, 605–609. https://doi.org/10.1038/nature02031

Rollinson, H. (2022) No plate tectonics necessary to explain Eoarchean rocks at Isua (Greenland). *Geology* 50, 147–151. https://doi.org/10.1130/G49278.1

Rzehak, L.J., Kommescher, S., Hoare, L., Kurzweil, F., Sprung, P., Leitzke, F.P., Fonseca, R.O. (2022) Redox-dependent Ti stable isotope fractionation on the Moon: implications for current lunar magma ocean models. *Contributions to Mineralogy and Petrology* 177, 81. https://doi.org/10.1007/s00410-022-01947-0

Saji, N.S., Rudnick, R.L., Gaschnig, R.M., Millet, M.-A. (2023) Titanium isotope evidence for the high topography of Nuna and Gondwana-Implications for Earth's redox and biological evolution. *Earth and Planetary Science Letters* 615, 118–214. https://doi.org/10.1016/j.epsl.2023.118214

Sizova, E., Gerya, T., Stüwe, K., Brown, M. (2015) Generation of felsic crust in the Archean: a geodynamic modeling perspective. *Precambrian Research* 271, 198–224. https://doi.org/10.1016/j.precamres.2015.10.005

Smithies, R., Champion, D., Van Krandendnk, M. (2009) Formation of Paleoarchean continental crust through infracrustal melting of enriched basalt. *Earth and Planetary Science Letters* 281, 298–306. https://doi.org/10.1016/j.epsl.2009.03.003

Zhang, C., Holtz, F., Koepke, J., Wolff, P.E., Ma, C., Bédard, J.H. (2013) Constraints from experimental melting of amphibolite on the depth of formation of garnet-rich restites, and implications for models of Early Archean crustal growth. *Precambrian Research* 231, 206–217. https://doi.org/10.1016/j.precamres.2013.03.004

Zhang, Z.J., Dauphas, N., Johnson, A.C., Aarons, S.M., Bennett, V.C., Nutman, A.P., MacLennan, S., Schoene, B. (2023) Titanium and iron isotopic records of granitoid crust production in diverse Archean cratons. *Earth and Planetary Science Letters* 620, 118342. https://doi.org/10.1016/j.epsl.2023.118342

Geochemical Perspectives Letters

Titanium isotope constraints on the mafic sources and geodynamic origins of Archean crust

L. Hoare, L.J.A. Rzehak, S. Kommescher, M. Jansen, M.T. Rosing, T. Nagel, M.-A. Millet, J. Elis Hoffmann, R.O.C. Fonseca

Supplementary Information

The Supplementary Information includes:

- 1. Samples
- 2. Methods
- 3. Thermodynamic Phase Equilibria Modelling
- 4. Trace Element Modelling
- 5. Modelling of Ti Isotope Fractionation
- Tables S-1 to S-11 (Tables S-2 to S-11 are available from the online version of this article at https://doi.org/10.7185/geochemlet.2342).
- Figures S-1 to S-4
- Supplementary Information References

1. Samples

All samples measured in this study have previously been characterised for their petrography, major and trace element compositions, and, in some instances radiogenic isotopes. Detailed geologic context, petrography, analytical methods, and major and trace element compositions of all tonalite and intracrustal differentiates can be found in Hoffmann *et al.* (2011a, b, 2014). The same information for all Isua tholeiitic metabasalt samples is sourced from Polat and Hofmann, 2003; Hoffmann *et al.*, 2011b. All geochemical data used in this study can be found in Tables S-3 to S-5 and S-9 to S-11. A brief outline of the sample petrography and major element geochemistry is provided below.

The mafic rocks analysed in this study consist of amphibolite facies tholeiitic to picritic metabasalts and metagabbros from the 3800 Ma (previously called the outer arc domain by Jenner *et al*., 2009) and 3700 Ma (referred to as the inner arc domain by Polat and Hofmann 2003) terranes within the Isua Supracrustal Belt (ISB) in southwest Greenland. The ISB mafic rocks exhibit low SiO_2 (45.9–54.5 wt. %), low TiO_2 (0.6–1.1 wt. %), low to moderate Al_2O_3 (7.9–14.2 wt. %), low to moderate Na_2O (0.3–3.7 wt. %), moderate to very high MgO (5.2–20.1 wt. %), low K_2O (0.01–1.40 wt. %) and Mg# from 46.1 to 75.4 (Table S-4). Igneous textures and minerals in these samples are not pre-served on the microscopic scale, and major mineral phases present include amphibole (hornblende, anthophyllite), plagioclase, chlorite, epidote, quartz, calcite, and titanite (*e.g*., Polat and Hofmann 2003; Hoffmann *et al.* 2011a, b).

All Itsaq Gneiss Complex (IGC) TTGs analysed in this study were collected in the Isukasia terrane in the southwest portion of the Isua Supracrustal Belt (ISB). The samples possess ages that range between 3650 to 3890 Ma (*e.g.*, Næraa *et al.*, 2012). Most IGC meta tonalite and trondhjemite samples in our study are well preserved and exhibit magmatic textures (*e.g.*, Nutman *et al.*, 1999; Hoffmann *et al.*, 2014). The main mineral assemblages of these rocks comprise plagioclase, quartz, amphibole, and biotite with minor titanite, apatite and accessory Fe-Ti oxides. The IGC meta tonalites and diorites exhibit moderate to high SiO_2 (62.0–72.9 wt. %), low TiO_2 (0.2–0.8 wt. %), high Al_2O_3 (14.8–18.1 wt. %), high Na_2O (4.0–5.9 wt. %), low to moderate MgO (0.5–3.2 wt. %), low to moderate K_2O (0.9–2.5 wt. %) and Mg# from 31.9 to 49.5 (Table S-5).

2. Methods

2.1. Chemical separation of Ti

For the duration of this study sample preparation first requires digestion of 20–60 mg (amount is dependent on the TiO_2 concentration of the sample to achieve at least 5 µg of natural Ti) of fine-powdered silicate rock sample or geo-standard in concentrated 1:1 mixture of HNO_3 and HF at 130 °C for 72 hours. An additional 2 ml of concentrated HNO_3 is then added and evaporated to incipient dryness. Following this step, each sample is taken up in 500 µl of concentrated HNO_3 and dried down, this step is repeated 3 times. The sample is then taken up in 6 M HCl with the addition of ~40 mg of H_3BO_3 into the solution to ensure the removal of any fluorides that would sequester Ti out of the sample solution. Finally, an aliquot containing 5 µg of Ti is taken from the sample solution and mixed with a ^{47}Ti-^{49}Ti double spike in a 48:52 ratio based on the calibration of Kommescher *et al.* (2020) and taken up in 5 mL 12 M HNO_3 prior to column chemistry.

Titanium is separated from the sample matrix using Eichrom N, N, N, N' tetra-n-octyldiglycolamide (DGA) resin. The procedure adopted in this study is based on the method initially developed by Zhang *et al.* (2011) and later modified by Hoare *et al.* (2020) and Millet *et al.* (2016). The method is outlined in Table S-1. This study used a double pass chemistry. Following purification, Ti fractions are treated with a 1:1 mixture of concentrated HNO_3 and 30 % H_2O_2 to remove any organic material.

Table S-1 Summary of ion exchange chromatography procedure for Ti purification of samples for MC- ICP-MS analysis

Step	Acid	Volume (mL)
Cleaning	Milli-Q	20
	3M HNO_3	10
Conditioning	12M HNO_3	10
Introduction	Sample in 12M HNO_3	5
Wash	12M HNO_3	20
Collect Ti	12M HNO_3 + 1 wt. % H_2O_2	10
Cleaning	Milli-Q	20
	3M HNO_3	10

2.2. Ti double spike MC-ICP-MS measurements and data reduction

Titanium isotope composition measurements of reference solutions OL-Ti and Col-Ti were carried out using a Nu Plasma II MC-ICP-MS at the Cardiff Earth Laboratory for Trace Element and Isotope Chemistry (CELTIC), School of Earth and Environmental Sciences, Cardiff University to check the double spike calibration. Samples and geo-reference materials were measured using either a Thermo Fischer Neptune XT MC-ICP-MS at the Deutsches Bergbau Museum, Bochum or a Thermo Fischer Neoma MC-ICP-MS at Freie Universität Berlin. For measurements on the Nu Plasma II samples were introduced via an Cetac Aridus II desolvating nebuliser (flushed with Ar), whereas in for sessions using a Themo Fischer Scientific Neptune and Neoma an ESI Apex Omega was used (flushed with Ar and N_2).

Prior to measurements purified samples were diluted to concentrations of 250 ng/g (Neptune XT and Neoma) or 1000 ng/g (Nu Plasma II) of Ti Samples were taken up in 0.3 M HNO_3 + 0.005 M HF solution. All instruments were fitted with nickel (Ni) jet-sampler and Ni (H) skimmer cones. The measurements were performed in medium resolution mode, with a resolution power (5-95 % peak definition, ΔM/M) in the range of ~ 5,000 or up to ~ 8,000 when using the Thermo Fischer Neoma MC-ICP-MS. Such resolution was sufficient to clearly identify the peak shoulders of the Ti isotopes, and simultaneously to counter the effect of non-resolvable polyatomic interferences such as $^{28}Si^{19}F$ and $^{14}N^{16}O_2H^+$ that can be introduced via the analyte solution (0.3 M HNO_3 – 0.005 M HF), which give inference on ^{47}Ti. The 'peak shoulder' is used to define an interference-free mass range on the respective mass, as polyatomic interferences are typically heavier than the respective mass. Titanium ion beam intensity ranged from 20-60 V on amplifiers with 10^{11} Ω resistors in their feedback loop. Ca interference on ^{46}Ti and ^{48}Ti was monitored at mass 44 and corrected during data reduction if necessary. Measurements of an individual sample consisted of 60-80 cycles with an integration time of 8 s. To account for small unresolved polyatomic interferences on ^{47}Ti due to the presence of F from the sample solution and Si from the torch ($^{28}Si^{19}F$), samples are bracketed by measurements of the double spiked OL-Ti standard solution.

The compositions of Ti reference solutions (OL-Ti and Col-Ti) and geo-reference materials (JB-2, BCR-2, AGV-1, G2) are in good agreement with previous published values (see Tables S-1 and S-2). The $\delta^{49/47}Ti$ value for AGV-1 reported here is heavier than the bulk of previously reported values but is within error of the recently published value of Storck *et al.* (2023; Table S-2) which could suggest this geo-reference standard is homogenous for Ti isotopes. Additionally, $\delta^{49/47}Ti$ values presented here for JA-2 and JG-2 differ from the values obtained by He *et al.* (2020; Table S-2). Given the lack of data for these two standards it is currently unclear if these offsets are the result of sample heterogeneity or inter laboratory bias. Further digestions and measurements of these geo reference materials will be required to confirm this. It should be noted that the samples ran on Neptune XT MC-ICP-MS at the Deutsches Bergbau Museum possess slightly larger 95 % c.i. values as during this session samples were analysed for fewer cycles (60 as opposed to 80). The 2σ internal precision of our $\delta^{49/47}Ti$ measurements, expressed as 95 % c.i. ssb (confidence interval; standard-sample-bracketing) is generally within ±0.020 - 0.030 ‰. The geo-reference materials and Ti reference solutions measured over the course of this study yield a pooled 2s intermediate precision of ±0.025 ‰, which we take as the best estimate of the uncertainty of our measurements. Total procedural blanks were always below 20 ng Ti, thus contributing less than 0.1% to the total processed sample Ti and are therefore negligible.

Table S-2 Summary of Ti isotope compositions of Ti reference solutions and geologic reference materials.

Reference solution/Geo-reference material	δ^{49}Ti (‰)	95 % c.i.	2 s.d.	n
OL-Ti	-0.010	0.004	0.025	32
Col-Ti	0.184	0.006	0.034	19
FUB-Ti (AA-Ti solution)	-0.162	0.006	0.034	12
BCR-2	-0.013	0.010	0.008	4
JB-2	-0.038	0.012	0.029	4
G-2	0.477	0.013	0.025	3
JA-2	0.137	0.020	-	1
AGV-2	0.134	0.018	-	1
JG-2	1.045	0.020	-	1

Table S-3 Summary of Ti isotope compositions of measured samples.

Sample	Rock type	δ^{49}Ti (‰)	95 % c.i.	2 s.d.	n
2000-10	Metabasalt	0.078	0.017	0.038	2
2000-13	Metabasalt	0.020	0.012	-	1
2000-4	Metabasalt	0.024	0.020	-	1
2000-6	Metabasalt	0.006	0.026	-	1
2000-7	Metabasalt	0.031	0.027	-	1
2000-8	Metabasalt	0.046	0.042	-	1
jeh-2007-11	Metabasalt	0.079	0.019	-	1
2007-01	Metagabbro	0.049	0.015	0.030	2
2007-08	Pillow basalt	0.040	0.016	0.013	2
2007-14	Sheeted dyke	0.084	0.018	0.016	2
2007-15	Sheeted dyke	0.051	0.017	0.040	2
229467	Pegmatitic white gneiss	1.105	0.020	-	1
498033	Augen gneiss	0.527	0.020	-	1
jeh-SG-07	migmatitic tonalite	0.246	0.018	-	1
498027	migmatitic tonalite	0.782	0.020	-	1
498028	migmatitic tonalite	0.382	0.019	-	1
229403	metadiorite	0.230	0.020	-	1
496430	non-gneissic tonalite	0.325	0.020	-	1
SG09	non-gneissic tonalite	0.444	0.016	0.040	2
499337	non-gneissic tonalite	0.294	0.020	-	1

496431	non-gneissic tonalite	0.417	0.022	-	1
SG10	non-gneissic tonalite	0.453	0.019	-	1
jeh-SG-01	non-gneissic tonalite	0.878	0.019	-	1
SG04	non-gneissic tonalite	0.377	0.021	-	1
SG05	non-gneissic tonalite	0.189	0.018	0.066	2
JEH-2007-05	non-gneissic tonalite	0.386	0.019	0.047	2
JEH 10–18	non-gneissic tonalite	0.361	0.017	0.054	2
JEH 10–19	non-gneissic tonalite	0.419	0.022	-	1
JEH 10–25	non-gneissic tonalite	0.352	0.019	-	1
JEH 10–38	non-gneissic tonalite	0.287	0.019	0.027	2
JEH 10–39	non-gneissic tonalite	0.273	0.020	0.070	2

3. Theriak-Domino Thermodynamic Phase Equilibria Modelling

To assess the extent of elemental and Ti isotope fractionation during partial melting of metabasalts and crystallisation of tonalitic melts we employ the use of constraints from the latest generation of phase equilibria modelling. The modelling uses the Theriak algorithm (de Capitani and Brown, 1987). which is implemented via the Domino software (de Capitani and Petrakakis, 2010). The current version of the Domino software used in this study is distributed on GitHub and can be accessed using the following link https://github.com/Theriak-Domino/theriak-domino/. The complete output from the models including run conditions, the compositions and proportions of phases can be found in Table S-6. The procedure for thermodynamic modelling adopted in this study closely follows that of Nagel *et al*. (2012) and Hoffmann *et al*. (2014).

The references for the databases and solution models for all phases are outlined below:

Database: Holland and Powell (2011)

Solution models:
Amphibole - Green *et al.* (2016)
Melt, ilmenite, rutile, clinopyroxene, orthopyroxene and garnet - Holland *et al.* (2018)
Plagioclase - Holland *et al.* (2022)
Mica - White *et al.* (2014)

Set up for Theriak-Domino: Jørgensen *et al.* (2019)

These data are combined with relevant mineral-melt trace element partition coefficients (Table S-7) and Ti isotope fractionation factors (Table S-8). This will quantitatively test if these processes are viable mechanisms to explain the range of elemental and $\delta^{49/47}$Ti compositions observed in ISB metabasalts and IGC tonalites.

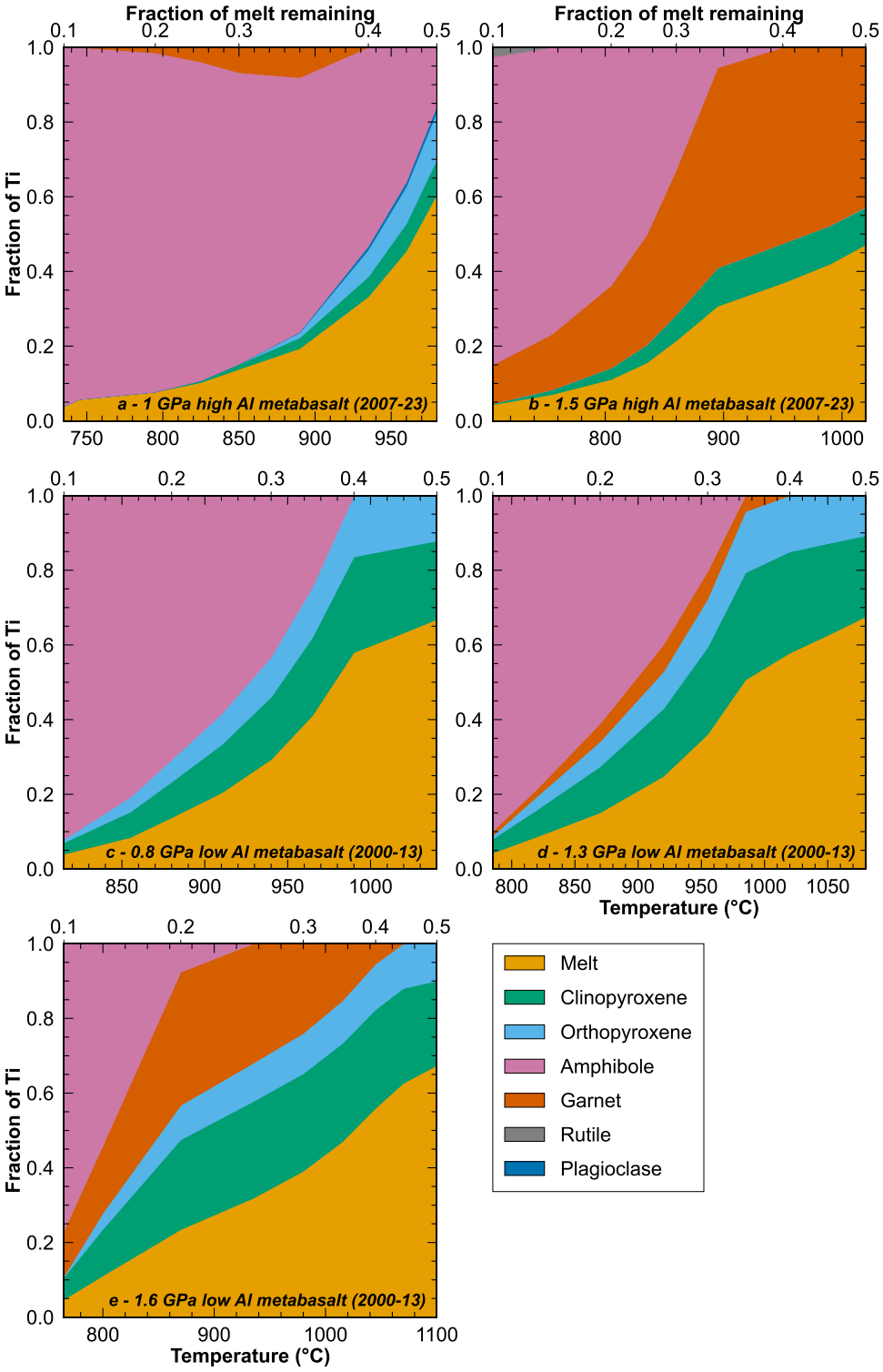

Figure S-1 Changes in the Titanium (Ti) budget of phases with respect to temperature and remaining melt fraction for partial melting of high-Al metabasalt sample 2007-23 at 1 GPa **(a);** and 1.5 GPa **(b)** and; low-Al metabasalt sample 2000-13 at 0.8 GPa **(c);** 1.3 GPa **(d);** and 1.6 GPa **(e)**.

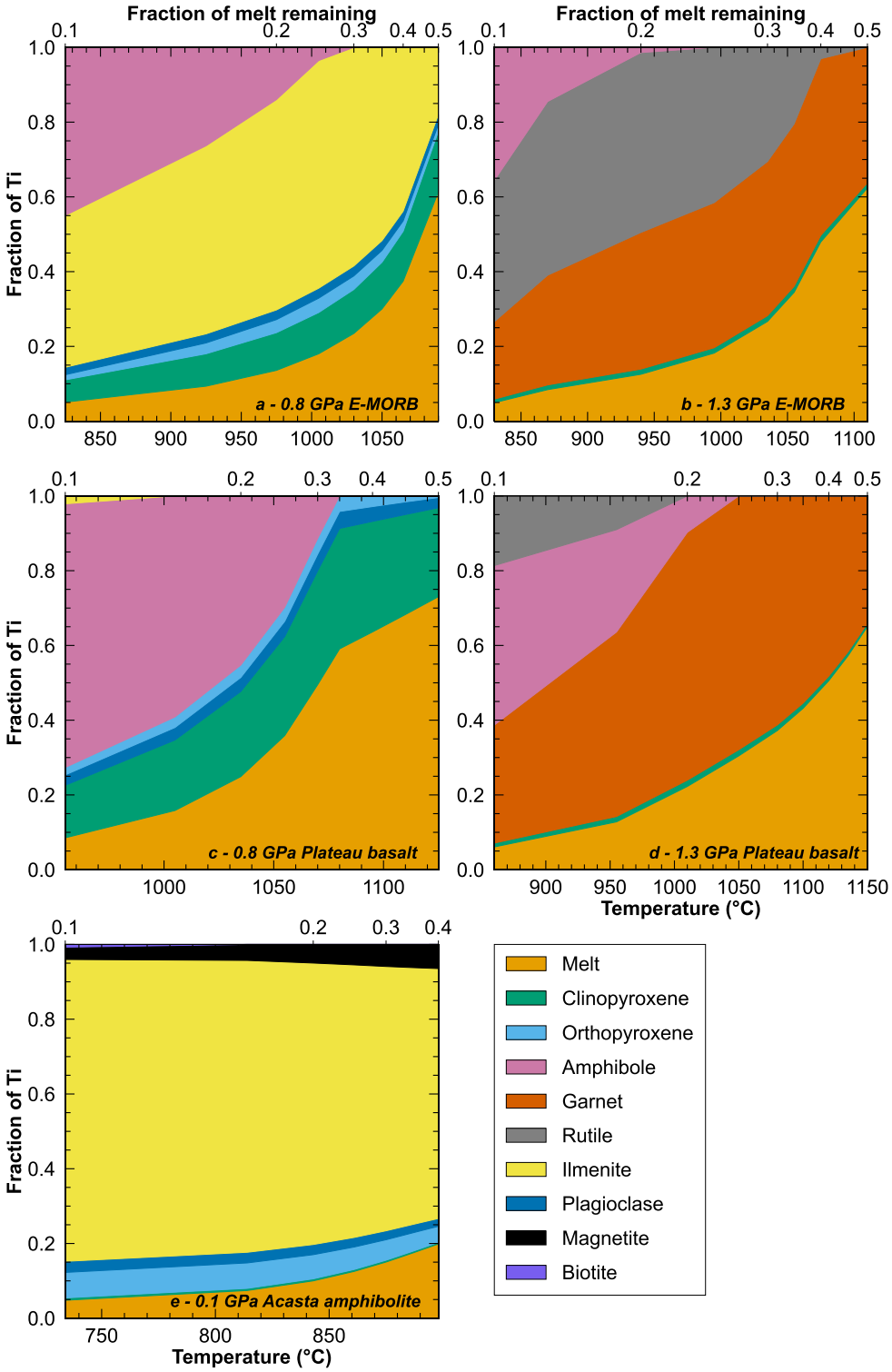

Figure S-2 Changes in the Titanium (Ti) budget of phases with respect to temperature and remaining melt fraction for partial melting of E-MORB (Gale *et al*., 2013) at 0.8 GPa **(a)** and 1.3 GPa **(b);** and a primitive flood basalt (Baffin island picrite; Kent *et al*., 2004) at 0.8 GPa **(c)** and 1.3 GPa **(d)**; and **(e)** an average Acasta amphibolite from (Johnson *et al*., 2018).

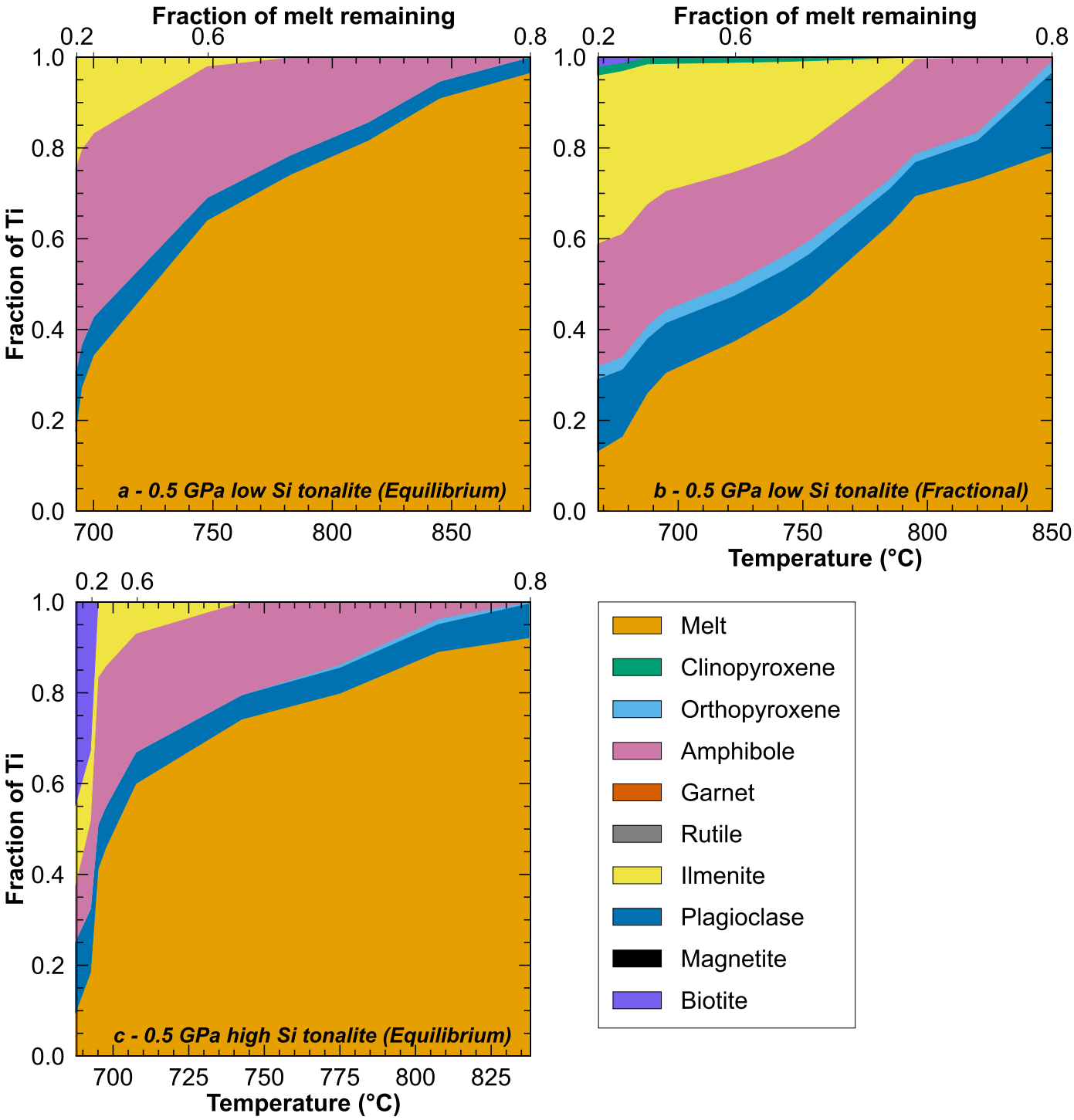

Figure S-3 Changes in the Titanium (Ti) budget of phases with respect to temperature and remaining melt fraction for equilibrium **(a)** and fractional **(b)** crystallisation of low-Si IGC tonalite sample G 97/31 at 0.5 GPa; and equilibrium crystallisation of IGC high-Si tonalite sample JEH 10-38 at 0.5 GPa **(c).**

Phase equilibria modelling is based on three scenarios using different mafic source compositions (see Table S-6, S-9, S-10). Firstly, hydrous partial melting of two metabasalts (high and low Al) representative of average compositions of local Eoarchean Isua mafic rocks (2007-23 - Hoffmann *et al.*, 2011b; 2000-13 - Polat and Hofmann, 2003), and then dehydration partial melting of E-MORB (Gale *et al.*, 2013), a picritic plateau basalt (Kent *et al.*, 2004), and an average amphibolite composition from the Acasta Gneiss complex (Johnson *et al.*, 2018). The initial H_2O contents used for the staring compositions was 4 wt. % and for Isua metabasalts, and 2 wt. % E-MORB and plateau basalt. The whole rock geochemistry of the starting compositions be found in Table S-6. Secondly, equilibrium and fractional crystallisation of two tonalite compositions (JEH 10-38 - Hoffmann *et al.*, 2011a; G97/31 - Nutman *et al.*, 1999). Amphibole is the dominant Ti-bearing mineral phase during partial melting of tholeiitic metabasalts (Fig. S-1, Tables S-6 and S-9), whereas depending on pressure, either ilmenite or rutile dominates during partial melting of E-MORB (Fig. S-2). Minor amounts Fe-Ti oxides only appear at low melt fraction (<10 %, Tables S-6 and S-9) for tholeiitic metabasalts (Table S-1 to 6). The distribution of Ti for low pressure (0.8 GPa) melting of a picritic plateau basalt is comparable to that of both tholeiitic metabasalts, except for minor amounts of ilmenite below 1000 °C, whereas at 1.3 GPa and below 1000 °C rutile hosts a significant portion of Ti (Figs. S-1, S-2). In stark contrast to the other partial melting models, ilmenite is the dominant Ti-bearing phase throughout the 0.1 GPa Acasta amphibolite model (Fig. S-2e, Table S-6, S-9). The appearance of amphibole and/or ilmenite causes the fraction of Ti hosted in the melt to sharply decline with decreasing melt fraction (Figs. S-1-3). Partial melting of the low-Al metabasalt produces plagioclase-free residues with clino- and orthopyroxene as the initially volumetrically dominant phases, until the appearance of amphibole below 1000 °C (Fig. S-1, Tables S-6 and S-9). Additionally, garnet is stabilised at ~ 1000 °C and 1050 °C at 1.3 and 1.6 GPa respectively in the low-Al metabasalt (Fig. S-1, Tables S-6, S-9) and at ~ 1100 °C for the high-Al metabasalt at 1.5 GPa (Fig. S-1, Table S-6, S-9). In the higher-pressure melting models garnet hosts a significant portion of Ti in the absence of amphibole or Fe-Ti oxides (Fig. S-1, S-2). Partial melting of high-Al metabasalt at 1 GPa produces plagioclase and notably less clinopyroxene compared to low-Al metabasalt (Fig. S-1, Tables S-6, S-9). Silicate melt is volumetrically dominant in the tonalite equilibrium and fractional crystallisation models, followed by plagioclase (Fig. S-3, Tables S-6, S-10). In the equilibrium models, amphibole, and biotite, along with minor amounts of ilmenite, quartz, and ortho- and clinopyroxene appear at lower temperature and melt fraction (Fig. S-3, Table S-6, S-10). In equilibrium crystallisation models, amphibole dominates the Ti budget of solid phases until the appearance of ilmenite, with biotite also sequestering a significant fraction of Ti at ~ 695 °C (Fig. S-3, Tables S-6, S-10). An abrupt transition occurs towards the latter stages of crystallisation (~ 80%) due to the appearance of biotite (Fig. S-3, Tables S-6, S-10), which dominates the Ti budget at low melt fraction (Fig. S-3, Tables S-6, S-10). The lower modal proportion of amphibole and earlier appearance of ilmenite in the fractional crystallisation model results in ilmenite being the dominant Ti-bearing phase (Fig. S-3, Table S-6, S-10). Clinopyroxene also possess a greater share of the Ti budget in comparison to the equilibrium models due to its higher modal abundance (Fig. S-3, Tables S-6, S-10).

4. Trace Element Modelling

For equilibrium partial melting and crystallisation models the trace element and Ti concentrations of the melt were calculated using the Equation S-1 (Shaw, 1970):

$$C_L = {}^{C_o}/_{D + F(1 - D)} \qquad \text{Eq. S-1}$$

where the trace-element composition of the liquid (C_L) depends on the composition of the source (C_0), the degree of partial melting (F), and the bulk distribution coefficient (D), itself a function of individual mineral partition coefficients

and mineral-melt proportions. The degree of melting, the residual mineral assemblage, and the associated mineral abundances are all controlled by the intensive and extensive chemical parameters (bulk composition, pressure, temperature, fluid pressure, oxygen fugacity etc.). Hence, this equation can be seen as relating C_L with (1) the nature of the mafic protolith and (2) the thermodynamic conditions of crustal evolution. This concept applies to melting and to crystallisation in the same way.

In fractional crystallisation scenarios a Rayleigh fractionation approach was used (Eq. S-2):

$$C_L = C_o D^{(1-F)} \qquad \text{Eq. S-2}$$

Trace element modelling always carries a certain degree of uncertainty, particularly in the case of TTG formation in which both amphibole and garnet are major residual phases (Foley, 2008; Qian and Hermann, 2013). The magnitude of D values in the literature for these phases varies greatly as function of pressure, temperature and melt composition, which is further compounded by the scarcity of experimental data relevant for tonalitic melts (Barth *et al.*, 2002; Foley, 2008; Klein *et al.*, 1997, 2000; Qian and Hermann, 2013). An effort was made to select experimentally determined mineral melt partition coefficients for tonalitic melts from the available published data at relevant pressure/temperature conditions (Barth *et al.*, 2002; Bédard, 2006; Klein *et al.*, 1997; Qian and Hermann, 2013). All mineral-melt partition coefficients ($D_{\text{min-melt}}$) used for trace element modelling are provided in Table S-7.

5. Modelling of Ti Isotope Fractionation

Equilibrium fractionation

Equilibrium isotope fraction during partial melting and crystallisation is governed by the following mass balance Equation S-3:

$$R^* = \frac{C_{melt}F_{melt}R_{melt}\alpha_{melt} + C_{amp}F_{amp}R_{melt}\alpha_{amp} + C_{cpx}F_{cpx}R_{melt}\alpha_{cpx} + \cdots}{C} \qquad \text{Eq. S-3}$$

In which R is an isotope ratio, $^{49}Ti/^{47}Ti$ in this case (relative to $^{49}Ti/^{47}Ti = 0.749766$ for OL-Ti), with a * used to represent the bulk composition. C is the concentration of Ti in a phase, F is the proportion of a phase, and α is the isotope fractionation factor between a given phase, (*i*) and the melt as defined by Equation S-4:

$$\alpha_i = \frac{R_i}{R_{melt}} \qquad \text{Eq. S-4}$$

The isotope mass balance equation can be rewritten as follows (Eq. S-5):

$$R^* = \frac{R_{melt}\sum_i (C_i F_i \alpha_i)}{C^*} \qquad \text{Eq. S-5}$$

If using mineral-melt partition coefficients the distribution of Ti (X_{Ti-i}) for each phase present can be calculated using (Eq. S-6):

$$X_{Ti-i} = \frac{F_i * D_{i-melt}^{Ti}}{\sum_n (F*D)} \qquad \text{Eq. S-6}$$

Finally, in instances where the bulk isotope composition is known, the isotope composition of the melt can be obtained using the Equation S-7:

$$R_{melt} = \frac{R^* C^*}{\sum_i (C_i F_i \alpha_i)} \qquad \text{Eq. S-7}$$

This equation was used to calculate the Ti isotope composition of melts produced during equilibrium melting and crystallisation. The isotope composition is reported relative to the Origins Lab Ti standard (Eq. S-8):

$$\delta^{49/47} Ti_{melt} = \left[\frac{R_{melt}}{R_{OL-Ti}}\right] - 1 \qquad \text{Eq. S-8}$$

Rayleigh fractionation

Ti isotope fractionation during tonalite fractional crystallisation was obtained using a Rayleigh fractionation law. The Ti isotope composition of fractionated melts was obtained using the following Equation S-9:

$$R_{melt} = R_o f^{\alpha - 1} \qquad \text{Eq. S-9}$$

where, R is the $^{49}Ti/^{47}Ti$ isotope ratio, R^o is the initial isotope ratio, f is the fraction of Ti remaining in the melt, and α is the bulk solid-melt isotope fractionation factor between the remaining melt and the crystallizing mineral assemblage, where the mineral-melt fractionation factors are weighted by their Ti concentration at each stage of the model.
All Ti mineral melt fractionation factors are reported in Table S-8. The references for each of the main Ti-bearing phases are outlined below:

Fe-Ti oxides (rutile, ilmenite, magnetite) - Hoare *et al.* (2022); Rzehak *et al.* (2022)
Amphibole, biotite and sphene - Mandl (2019)
Clinopyroxene - Rzehak *et al.* (2022)
Orthopyroxene - Rzehak *et al.* (2021)
Garnet - Wang *et al.* (2020)

The phase proportions and Ti content of each phase are provided by the thermodynamic phase equilibria modelling for partial melting of metabasalts and tonalite crystallisation. In the case of partial melting models, the revised value of the bulk silicate Earth of +0.05 ± 0.01 ‰ from the recent study of Deng *et al.* (2023) was used as the initial bulk Ti isotope composition, which is indistinguishable from the weighted mean of the Isua metabasalts presented in this study ($\delta^{49/47}Ti$ = +0.052 ± 0.006 ‰; 95% c.i; n = 11). For tonalite crystallisation, the Ti isotope composition of JEH 10-38 was used (Table S-5). Whereas $\delta^{49/47}Ti$ composition of tonalite sample G97/31 was estimated via an exponential function of SiO_2 vs $\delta^{49/47}Ti$ using published data for Archean amphibolites and TTGs (n=48). The exponential function $\delta^{49/47}Ti = 2.3*10^{-}$

$^{4} * e^{1.04*10-1}$ ($R^2 = 0.85$) yielded a value of +0.23 ‰ for an SiO_2 content of 66.79 wt. % (Tables S-4, S-5, and S-11). This value is comparable to other TTG samples of similar SiO_2 contents (*e.g.* G91/61; Zhang *et al.*, 2023, Table S-11).

Supplementary Tables

Tables S-2 to S-11 are available for download (.xls) from the online version of this article at https://doi.org/10.7185/geochemlet.2342.

Table S-1 see page SI-2

Table S-2 see page SI-4

Table S-3 see pages SI-4 and SI-5

Table S-4 Whole rock geochemistry and Ti isotope compositions of Isua supracrustal belt metabasalts measured in this study.

Table S-5 Whole rock geochemistry and Ti isotope compositions of Itsaq Gneiss Complex samples measured in this study.

Table S-6 Results and output of Theriak/Domino phase equilibria modelling.

Table S-7 Mineral-melt partition coefficients and source compositions used for trace element modelling during partial melting and crystallisation.

Table S-8 Mineral-melt titanium isotope fractionation factors used for modelling of Ti isotope fractionation during partial melting and crystallisation.

Table S-9 Results of trace element and Ti isotope modelling for metabasalt partial melting.

Table S-10 Results of trace element and Ti isotope modelling for tonalite differentiation.

Table S-11 Compilation of literature whole rock geochemical data used in this study.

Supplementary Information References

Aarons, S.M., Reimink, J.R., Greber, N.D., Heard, A.W., Zhang, Z., Dauphas, N. (2020) Titanium isotopes constrain a magmatic transition at the Hadean-Archean boundary in the Acasta Gneiss Complex. *Science Advances* 6, eabc9959. https://doi.org/10.1126/sciadv.abc9959

Barling, J., Goldstein, S.L., Nicholls, I.A. (1994) Geochemistry of Heard Island (southern Indian Ocean): Characterization of an enriched mantle component and implications for enrichment of the sub-Indian Ocean mantle. *Journal of Petrology* 35,1017–1053. https://doi.org/10.1093/petrology/35.4.1017

Barth, M.G., Foley, S.F., Horn, I. (2002) Partial melting in Archean subduction zones: constraints from experimentally determined trace element partition coefficients between eclogitic minerals and tonalitic melts under upper mantle conditions. *Precambrian Research* 113, 323–340. https://doi.org/10.1016/S0301-9268(01)00216-9

Bédard, J.H. (2006) A catalytic delamination-driven model for coupled genesis of Archaean crust and sub-continental lithospheric mantle. *Geochimica et Cosmochimica Acta* 70, 1188–1214. https://doi.org/10.1016/j.gca.2005.11.008

de Capitani, C., Brown, T.H. (1987) The computation of chemical equilibrium in complex systems containing non-ideal solutions. *Geochimica et Cosmochimica Acta* 51, 2639–2652. https://doi.org/10.1016/0016-7037(87)90145-1

de Capitani, C., Petrakakis, K. (2010) The computation of equilibrium assemblage diagrams with Theriak/Domino software. *American Mineralogist* 95, 1006–1016. https://doi.org/10.2138/am.2010.3354

Chamberlain, K.J., Barclay, J., Preece, K.J., Brown, R.J., Davidson, J.P. (2019) Lower crustal heterogeneity and fractional crystallization control evolution of small-volume magma batches at ocean island volcanoes (Ascension Island, South Atlantic). *Journal of Petrology* 60, 489-1522. https://doi.org/10.1093/petrology/egz037

Clague, D.A., Caress, D.W., Dreyer, B.M., Lundsten, L., Paduan, J.B., Portner, R.A., Spelz‐Madero, R., Bowles, J.A., Castillo, P.R., Guardado‐France, R., Le Saout, M. (2018) Geology of the Alarcon Rise, southern Gulf of California. *Geochemistry, Geophysics, Geosystems* 19, 807-837. https://doi.org/10.1002/2017GC007348

Dempsey, S. (2013) *Geochemistry of volcanic rocks from the Sunda Arc* (Doctoral dissertation, Durham University).

Deng, Z., Moynier, F., Sossi, P.A., Chaussidon, M. (2018) Bridging the depleted MORB mantle and the continental crust using titanium isotopes. *Geochemical Perspectives Letters* 9, 11-15. https://doi.org/10.7185/geochemlet.1831

Deng, Z., Chaussidon, M., Savage, P., Robert, F., Pik, R., Moynier, F. (2019) Titanium isotopes as a tracer for the plume or island arc affinity of felsic rocks. *Proceedings of the National Academy of Sciences*, 116, 1132–1135. https://doi.org/10.1073/pnas.1809164116

Deng, Z., Schiller, M., Jackson, M.G., Millet, M.A., Pan, L., Nikolajsen, K., Saji, N.S., Huang, D., Bizzarro, M. (2023) Earth's evolving geodynamic regime recorded by titanium isotopes. *Nature* 621, 100-104. https://doi.org/10.1038/s41586-023-06304-0

Foley, S. (2008) A trace element perspective on Archean crust formation and on the presence or absence of Archean subduction. In: Condie, K.C., Pease, V. *When did plate tectonics begin on planet Earth? Geological Society of America* 440, 31. https://doi.org/10.1130/2008.2440(02)

Gale, A., Dalton, C.A., Langmuir, C.H., Su, Y., Schilling, J. (2013) The mean composition of ocean ridge basalts. *Geochemistry, Geophysics, Geosystems* 14, 489–518. https://doi.org/10.1029/2012GC004334

Greber, N.D., Dauphas, N., Bekker, A., Ptáček, M.P., Bindeman, I.N., Hofmann, A. (2017) Titanium isotopic evidence for felsic crust and plate tectonics 3.5 billion years ago. *Science* 357, 1271-1274. https://doi.org/10.1126/science.aan8086

Greber, N.D., Pettke, T., Vilela, N., Lanari, P., Dauphas, N. (2021) Titanium isotopic compositions of bulk rocks and mineral separates from the Kos magmatic suite: Insights into fractional crystallization and magma mixing processes. *Chemical Geology* 578, 120303. https://doi.org/10.1016/j.chemgeo.2021.120303

Green, E., White, R., Diener, J., Powell, R., Holland, T., Palin, R. (2016) Activity–composition relations for the calculation of partial melting equilibria in metabasic rocks. *Journal of Metamorphic Geology* 34, 845–869. https://doi.org/10.1111/jmg.12211

He, X., Ma, J., Wei, G., Zhang, L., Wang, Z., Wang, Q. (2020) A new procedure for titanium separation in geological samples for 49 Ti/47 Ti ratio measurement by MC-ICP-MS. *Journal of Analytical Atomic Spectrometry* 35, 100–106. https://doi.org/10.1039/C9JA00316A

He, X., Ma, J., Wei, G., Wang, Z., Zhang, L., Zeng, T., Zhang, Z., (2022) Mass-dependent fractionation of titanium stable isotopes during intensive weathering of basalts. *Earth and Planetary Science Letters* 579, 117347. https://doi.org/10.1016/j.epsl.2021.117347

Hoare, L., Klaver, M., Saji, N.S., Gillies, J., Parkinson, I.J., Lissenberg, C.J., Millet, M.-A. (2020) Melt chemistry and redox conditions control titanium isotope fractionation during magmatic differentiation. *Geochimica et Cosmochimica Acta* 282, 38–54. https://doi.org/10.1016/j.gca.2020.05.015

Hoare, L., Klaver, M., Muir, D.D., Klemme, S., Barling, J., Parkinson, I.J., Lissenberg, C.J., Millet, M.-A. (2022) Empirical and experimental constraints on Fe-Ti oxide-melt titanium isotope fractionation factors. *Geochimica et Cosmochimica Acta* 326, 253–272. https://doi.org/10.1016/j.gca.2022.02.011

Hoffmann, J.E., Münker, C., Næraa, T., Rosing, M.T., Herwartz, D., Garbe-Schönberg, D., Svahnberg, H. (2011a) Mechanisms of Archean crust formation inferred from high-precision HFSE systematics in TTGs. *Geochimica et Cosmochimica Acta* 75, 4157–4178. https://doi.org/10.1016/j.gca.2011.04.027

Hoffmann, J.E., Münker, C., Polat, A., Rosing, M.T., Schulz, T. (2011b) The origin of decoupled Hf–Nd isotope compositions in Eoarchean rocks from southern West Greenland. *Geochimica et Cosmochimica Acta* 75, 6610–6628. https://doi.org/10.1016/j.gca.2011.08.018

Hoffmann, J.E., Nagel, T.J., Muenker, C., Naeraa, T., Rosing, M.T. (2014) Constraining the process of Eoarchean TTG formation in the Itsaq Gneiss Complex, southern West Greenland. *Earth and Planetary Science Letter*s 388, 374–386. https://doi.org/10.1016/j.epsl.2013.11.050

Holland, T., Powell, R. (2011) An improved and extended internally consistent thermodynamic dataset for phases of petrological interest, involving a new equation of state for solids. *Journal of metamorphic Geology* 29, 333–383. https://doi.org/10.1111/j.1525-1314.2010.00923.x

Holland, T.J., Green, E.C., Powell, R. (2018) Melting of peridotites through to granites: a simple thermodynamic model in the system KNCFMASHTOCr. *Journal of Petrology* 59, 881–900. https://doi.org/10.1093/petrology/egy048

Holland, T.J.B., Green, E.C.R., Powell, R. (2022) A thermodynamic model for feldspars in KAlSi3O8− NaAlSi3O8− CaAl2Si2O8 for mineral equilibrium calculations. *Journal of Metamorphic Geology* 40, 587–600. https://doi.org/10.1111/jmg.12639

Jenner, F.E., Bennett, V.C., Nutman, A.P., Friend, C.R.L., Norman, M.D., Yaxley, G. (2009) Evidence for subduction at 3.8 Ga: geochemistry of arc-like metabasalts from the southern edge of the Isua Supracrustal Belt. *Chemical Geology* 261, 83–98. https://doi.org/10.1016/j.chemgeo.2008.09.016

Johnson, T.E., Gardiner, N.J., Miljković, K., Spencer, C.J., Kirkland, C.L., Bland, P.A., Smithies, H. (2018) An impact melt origin for Earth's oldest known evolved rocks. *Nature Geoscience* 11, 795–799. https://doi.org/10.1038/s41561-018-0206-5

Jørgensen, T.R., Tinkham, D.K., Lesher, C.M. (2019) Low‐P and high‐T metamorphism of basalts: Insights from the Sudbury impact melt sheet aureole and thermodynamic modelling. *Journal of Metamorphic Geology* 37, 271–313. https://doi.org/10.1111/jmg.12460

Kent, A., Stolper, E., Francis, D., Woodhead, J., Frei, R., Eiler, J. (2004) Mantle heterogeneity during the formation of the North Atlantic igneous province: Constraints from trace element and Sr‐Nd‐Os‐O isotope systematics of Baffin Island picrites. *Geochemistry, Geophysics, Geosystems* 5. https://doi.org/10.1029/2004GC000743

Klaver, M., Carey, S., Nomikou, P., Smet, I., Godelitsas, A., Vroon, P. (2016) A distinct source and differentiation history for Kolumbo submarine volcano, Santorini volcanic field, Aegean arc. *Geochemistry, Geophysics, Geosystems*, 17, 3254-3273. https://doi.org/10.1002/2016GC006398

Klaver, M., MacLennan, S.A., Ibañez-Mejia, M., Tissot, F.L., Vroon, P.Z., Millet, M.A. (2021) Reliability of detrital marine sediments as proxy for continental crust composition: The effects of hydrodynamic sorting on Ti and Zr isotope systematics. *Geochimica et Cosmochimica Acta* 310, 221-239. https://doi.org/10.1016/j.gca.2021.05.030

Klein, M., Stosch, H.-G., Seck, H. (1997) Partitioning of high field-strength and rare-earth elements between amphibole and quartz-dioritic to tonalitic melts: an experimental study. *Chemical Geology*. 138, 257–271. https://doi.org/10.1016/S0009-2541(97)00019-3

Klein, M., Stosch, H.-G., Seck, H., Shimizu, N. (2000) Experimental partitioning of high field strength and rare earth elements between clinopyroxene and garnet in andesitic to tonalitic systems. *Geochimica et Cosmochimica Acta*. 64, 99–115. https://doi.org/10.1016/S0009-2541(97)00019-3

Kommescher, S., Fonseca, R.O.C., Kurzweil, F., Thiemens, M.M., Münker, C., Sprung, P. (2020) Unravelling lunar mantle source processes via the Ti isotope composition of lunar basalts. *Geochemical Perspectives Letters* 13, 13–18. https://doi.org/10.7185/geochemlet.2007

Li, J., Tang, S., Zhu, X., Ma, J., Zhao, X. (2022) Titanium Isotope Analysis of Igneous Reference Materials using a Double‐spike MC‐ICP‐MS Method. *Acta Geologica Sinica‐English Edition* 96, 517-524. https://doi.org/10.1111/1755-6724.14728

Mancini, A., Mattsson, H.B., Bachmann, O. (2015) Origin of the compositional diversity in the basalt-to-dacite series erupted along the Heiðarsporður ridge, NE Iceland. *Journal of Volcanology and Geothermal Research*, 301, 116-127. https://doi.org/10.1016/j.jvolgeores.2015.05.010

Mandl, M.B. (2019) Titanium isotope fractionation on the Earth and moon: constraints on magmatic processes and moon formation. Doctoral dissertation, ETH Zurich.

Millet, M.-A., Dauphas, N., Greber, N.D., Burton, K.W., Dale, C.W., Debret, B., Macpherson, C.G., Nowell, G.M., Williams, H.M. (2016) Titanium stable isotope investigation of magmatic processes on the Earth and Moon. *Earth and Planetary Science Letters*. 449, 197–205. https://doi.org/10.1016/j.epsl.2016.05.039

Millet, M.A., Dauphas, N. (2014) Ultra-precise titanium stable isotope measurements by double-spike high resolution MC-ICP-MS. *Journal of Analytical Atomic Spectrometry*, 29, 1444–1458. https://doi.org/10.1039/C4JA00096J

Naeraa, T., Scherstén, A., Rosing, M.T., Kemp, A.I.S., Hoffmann, J.E., Kokfelt, T.F., Whitehouse, M.J. (2012) Hafnium isotope evidence for a transition in the dynamics of continental growth 3.2 Gyr ago. *Nature* 485, 627-630. https://doi.org/10.1038/nature11140

Nagel, T.J., Hoffmann, J.E., Münker, C. (2012) Generation of Eoarchean tonalite-trondhjemite-granodiorite series from thickened mafic arc crust. *Geology* 40, 375–378. https://doi.org/10.1130/G32729.1

Nash, W.P., Crecraft, H.R. (1985) Partition coefficients for trace elements in silicic magmas. *Geochimica et Cosmochimica Acta* 49, 2309-2322. https://doi.org/10.1016/0016-7037(85)90231-5

Nutman, A.P., Bennett, V.C., Friend, C.R., Norman, M.D. (1999) Meta-igneous (non-gneissic) tonalites and quartz-diorites from an extensive ca. 3800 Ma terrain south of the Isua supracrustal belt, southern West Greenland: constraints on early crust formation. *Contributions to Mineralogy and Petrology* 137, 364–388. https://doi.org/10.1007/s004100050556

Polat, A., Hofmann, A. (2003) Alteration and geochemical patterns in the 3.7–3.8 Ga Isua greenstone belt, West Greenland. *Precambrian Research* 126, 197–218. https://doi.org/10.1016/S0301-9268(03)00095-0

Qian, Q., Hermann, J. (2013) Partial melting of lower crust at 10–15 kbar: constraints on adakite and TTG formation. *Contributions to Mineralogy and Petrology* 165, 1195–1224. https://doi.org/10.1007/s00410-013-0854-9

Rzehak, L.J.A., Kommescher, S., Kurzweil, F., Sprung, P., Leitzke, F.P., Fonseca, R.O.C. (2021) The redox dependence of titanium isotope fractionation in synthetic Ti-rich lunar melts. *Contributions to Mineralogy and Petrology* 176, 1–16. https://doi.org/10.1007/s00410-020-01769-y

Rzehak, L.J., Kommescher, S., Hoare, L., Kurzweil, F., Sprung, P., Leitzke, F.P., Fonseca, R.O. (2022) Redox-dependent Ti stable isotope fractionation on the Moon: implications for current lunar magma ocean models. *Contributions to Mineralogy and Petrology* 177, 81. https://doi.org/10.1007/s00410-022-01947-0

Savage, P.S., Georg, R.B., Williams, H.M., Burton, K.W., Halliday, A.N. (2011) Silicon isotope fractionation during magmatic differentiation. *Geochimica et Cosmochimica Acta* 75, 6124-6139. https://doi.org/10.1016/j.gca.2011.07.043

Shaw, D.M. (1970) Trace element fractionation during anatexis. *Geochimica et Cosmochimica Acta*. 34, 237–243. https://doi.org/10.1016/0016-7037(70)90009-8

Storck, J.-C., Greber, N.D., Duarte, J.F.V., Lanari, P., Tiepolo, M., Pettke, T. (2023) Molybdenum and titanium isotopic signatures of arc-derived cumulates. *Chemical Geology* 617, 121260. https://doi.org/10.1016/j.chemgeo.2022.121260

Szymanowski, D., Ellis, B.S., Wotzlaw, J.F., Bachmann, O. (2019) Maturation and rejuvenation of a silicic magma reservoir: High-resolution chronology of the Kneeling Nun Tuff. *Earth and Planetary Science Letters* 510, 103-115. https://doi.org/10.1016/j.epsl.2019.01.007

Timm, C., Graham, I.J., de Ronde, C.E., Leybourne, M.I., Woodhead, J. (2011) Geochemical evolution of Monowai volcanic center: New insights into the northern Kermadec arc subduction system, SW Pacific. *Geochemistry, Geophysics, Geosystems* 12. https://doi.org/10.1029/2011GC003654

Wang, W., Huang, S., Huang, F., Zhao, X., Wu, Z. (2020) Equilibrium inter-mineral titanium isotope fractionation: Implication for high-temperature titanium isotope geochemistry. *Geochimica et Cosmochimica Acta* 269, 540–553. https://doi.org/10.1016/j.gca.2019.11.008

Wanke, M., Karakas, O., Bachmann, O. (2019) The genesis of arc dacites: the case of Mount St. Helens, WA. *Contributions to Mineralogy and Petrology* 174, 1–14. https://doi.org/10.1007/s00410-018-1542-6

White, R., Powell, R., Holland, T., Johnson, T., Green, E. (2014) New mineral activity–composition relations for thermodynamic calculations in metapelitic systems. *Journal of Metamorphic Geology* 32, 261–286. https://doi.org/10.1111/jmg.12071

Williams, N.H. (2015) Titanium isotope cosmochemistry. Doctoral dissertation, University of Manchester.

Williams, N.H., Fehr, M.A., Parkinson, I.J., Mandl, M.B., Schönbächler, M. (2021) Titanium isotope fractionation in solar system materials. *Chemical Geology* 568, 120009. https://doi.org/10.1016/j.chemgeo.2020.120009

Xiong, X.L. (2006) Trace element evidence for growth of early continental crust by melting of rutile-bearing hydrous eclogite. *Geology* 34, 945-948. https://doi.org/10.1130/G22711A.1

Zhang, J., Dauphas, N., Davis, A.M., Pourmand, A. (2011) A new method for MC-ICPMS measurement of titanium isotopic composition: Identification of correlated isotope anomalies in meteorites. *Journal of Analytical Atomic Spectrometry* 26, 2197–2205. https://doi.org/10.1039/c1ja10181a

Zhang, Z.J., Dauphas, N., Johnson, A.C., Aarons, S.M., Bennett, V.C., Nutman, A.P., MacLennan, S., Schoene, B. (2023) Titanium and iron isotopic records of granitoid crust production in diverse Archean cratons. *Earth and Planetary Science Letters* 620, 118342. https://doi.org/10.1016/j.epsl.2023.118342